IOP Publishing Journal of Physics D: Applied Physics
J. Phys. D: Appl. Phys. **57** (2024) 355302 (16pp) https://doi.org/10.1088/1361-6463/ad4a84

Effect of carbon dots on tuning molecular alignment, dielectric and electrical properties of a smectogenic cyanobiphenyl-based liquid crystal material

Priscilla P[1], Sandeep Kumar[2,3], Arvind K Gathania[4], Ashwani Kumar Singh[5], Supreet[6], Jai Prakash[7], Sanjeev Kumar[8], Praveen Malik[5,*], Riccardo Castagna[9,10] and Gautam Singh[1,*]

[1] Department of Applied Physics, Amity Institute of Applied Sciences, Amity University Uttar Pradesh, Noida 201313, India
[2] Raman Research Institute, C V Raman Avenue, Sadashivanagar, Bengaluru 560080, India
[3] Department of Chemistry, Nitte Meenakshi Institute of Technology, Yelahanka, Bengaluru 560064, India
[4] Department of Physics and Photonic Science, National Institute of Technology, Hamirpur, Himachal Pradesh 177005, India
[5] Liquid Crystal Lab, Department of Physics, Dr B R Ambedkar National Institute of Technology, Jalandhar 144805, India
[6] Department of Physics, Amity School of Applied Sciences, Amity University, Haryana 122413, India
[7] Department of Physics, Aligarh Muslim University, Aligarh 202002, India
[8] Department of Physics, Chandigarh University-Gharuan, Mohali 140413, India
[9] CNR, Institute of Heritage Science, Via Madonna del Piano, 50019 Sesto Fiorentino, FI, Italy
[10] URT-CNR, Universit'a di Camerino (UNICAM), Polo di Chimica, Via Sant'Agostino, 1, 62032 Camerino, MC, Italy

E-mail: malikp@nitj.ac.in and gsingh6@amity.edu

Received 7 March 2024, revised 14 April 2024
Accepted for publication 13 May 2024
Published 10 June 2024

Abstract

Here, we demonstrate the effect of dispersing organosoluble carbon dots (CDs, ∼7–8 nm) on tuning the molecular alignment, dielectric and electrical properties of smectic A (SmA) and nematic (N) mesophases of a thermotropic smectogenic LC material, 4-octyl-4′-cyanobiphenyl (8CB) in a planar anchored indium tin oxide (ITO) sample cell using polarized optical microscopy and dielectric spectroscopic techniques. The cross-polarized optical textures clearly show that the doping of CDs (concentration ⩾0.25 wt%) in planar anchored 8CB liquid crtstal (LC) led to the changing of its alignment from planar to vertical. Interestingly, such an induced vertical alignment remains stable throughout the SmA and N phases of the 8CB LC material. Moreover, the magnitude of the real dielectric permittivity is found to increase with increasing concentration of CDs and exhibits vertical alignment values for composites (⩾0.25 wt%). The observance of short axis molecular relaxation for composites (⩾0.25 wt%) without the application of bias field confirms again the induced vertical alignment. The accumulation of CDs at the substrate surface

* Authors to whom any correspondence should be addressed.

and their interaction with the alignment and ITO layers can be attributed as an important factor for such induced vertical alignment. The electrical conductivity of 8CB is observed to increase significantly with the addition of CDs (i.e. an increment of up to two orders of magnitude in composites compared to pure 8CB) and attributed to the lowering of viscosity and change in molecular alignment. We certainly believe that such tunable molecular alignment throughout the SmA and N phases of thermotropic smectogenic LC material (8CB) by dopant CDs could pave the way for their applications in flexible displays, biosensors, electro-optical memory and other tunable photonic devices.

Supplementary material for this article is available online

Keywords: thermotropic liquid crystals, carbon dots, alignment, optical polarizing microscopy, dielectric spectroscopy

1. Introduction

Liquid crystal (LC), a widely popular intermediate state of matter existing between crystalline solids and isotropic liquids, has developed to become one of the most alluring soft matter systems [1, 2]. Its sensitivity to temperature revealed the various subphases that can be categorized according to its ordering structure. For instance, nematic LC (NLC) is the simplest of all the LC phases and most prevalent in our modern life due to its quicker response to external stimuli and its self-assembling nature. In nematic (N) phase, molecules tend to align themselves along a common direction, i.e. director (**n**) [3, 4]. Inclusion of a 1D positional ordering in the existing long-range orientational ordering of the N phase would create another subphase popularly known as the Smectic A (SmA) phase. The ability of the LC to showcase fascinating yet tailorable ordered superstructures that are highly sensitive to external stimuli makes it an unfailing paradigm in the display industry [5]. It is worth pointing out here that the application of LCs is not just limited to display industries [6–9] since its ease of forming varied material structures makes them ideal for biosensing [10], drug delivery [11], microlensing [12, 13], tuneable lasers [14], photonic crystals [15], vortex beam generators [16], etc. However, certain limitations, such as the lack of gray-scale capability, low contrast ratio, narrow viewing angle, lower light efficiency, requirement of backlight sources, high-power consumption, etc [17, 18] have often remained as a bottleneck that researchers time and again have attempted to resolve utilizing a variety of techniques. The dispersion of nanoparticles (NPs, particles with at least one dimension less than 100 nm) in LCs is one such technique that has yielded significant curiosity in the scientific community due to the intriguing and purposeful results that it produces [19–36]. Among NPs, quantum dots (QDs) are well probed due to their miniature size that ranges from 2–10 nm [37–39]. QDs in LCs have proven to be the most efficient kind of dispersion as it helps in manipulating optical, electro-optical and dielectric properties of LC materials [40]. For instance, Cd-based QDs (e.g. CdS, CdSe, CdSe/ZnS, etc.) have been utilized by researchers for enhancing the LC properties [41]. However, due to toxicity issues, nowadays scientists are switching over to eco-friendly QDs [41–43]. Research on eco-friendly QDs is accelerating since they are friendly both to human health and the environment. Within this framework, the carbon dot (CD) is recognized to be one such ecological dot that is in limelight these days [44, 45]. High electron conductivity, fluorescence, high photoluminescent quantum yield, great solubility in aqueous media, resistance to photobleaching and photo-decomposition, tuneable excitation and emission range, cost-effectiveness, etc, are just some of the wide-ranging characteristics found in CDs [46, 47]. Not only are they able to retain the properties of conventional semiconductor QDs, but they are also able to compensate their drawbacks in terms of environmental impact, toxicity and biohazards [48].

Coalescence of CDs with LCs has attracted significant attention recently since it was able to illustrate various enhancements and tailoring the properties of LCs in a range of studies conducted by researchers [49]. Most of the research is primarily concerned with NLCs, and they investigate how CDs modify their alignment, dielectric, electro-optical, thermal and non-linear optical characteristics. In this regard, a Turkish-based researcher studied the thermal and electro-optical properties of NLC (E7) dispersed with eco-friendly water-soluble CDs and reported an increased threshold voltage and elastic constant, but reduced clearing temperature ($T_{N\text{-}I}$) [50]. Further exploration on the CDs effect by the Manohar group demonstrated that doping of oil palm leaf-based porous CDs in NLC (E 48) resulted in faster switching response time, enhanced memory effect and reduced rotational viscosity [51]. In addition, they confirmed the formation of stable composites through zeta potential, enhanced molecular alignment, increased dielectric strength and relaxation and decreased activation energy as some of the main variations [52]. Recently, the Manohar group also demonstrated the modulation in the birefringence, contrast ratio, threshold voltage and dielectric properties of NLC (ZLI 2222–000) by doping CDs [53]. The authors predicted the use of these nanocomposites in LC displays and other opto-electronic devices such as tunable retarders. Induction of vertical alignment in NLC

(5CB) filled in a planar anchored sample cell by the doping of organosoluble CDs has recently been reported by our group [54, 55]. Quenching of the photoluminescence intensity, reduction in UV–vis absorbance at lower wavelengths and an increased zeta potential have been reported by Pandey *et al* [56] in CDs-NLC (7CB) composites. They further explored the effect of CDs on NLC (E 48) using time-resolved fluorescence spectroscopy, and observed a lack of Förster resonance energy transfer in all composites, UV–vis absorbance revealed a redshift at 0 V and a blue-shift at 10 V due to the molecular interaction between CDs and NLC [57]. Delving into a distinctive regime, the Varghese group [58] investigated the effect of organophilic CDs on third-order non-linear optical features of NLC (5PCH) and reported a significant improvement in both non-linear absorption and refraction coefficients apparently attributed to the Janossy effect and charge transfer mechanism. The authors pointed out that these CDs-NLC composites would certainly be useful for nonlinear photonic devices and optical limiters.

To the best of our knowledge, there is only one report from the Hegmann group, which talks about doping of CDs in LC material (Felix-2900–03) having both SmA and N phases [59]. They examined the effect of varying concentration of CDs (0.5–5.0 wt%) on the pre-existing planar alignment (planar anchored sample cells) and physical properties of LC. The reduction in elastic constant, apparent threshold voltage and dielectric anisotropy, but increment in rotational viscosity of the N phase of LC material with increase in concentration of CDs were observed. Interestingly, the planar alignment of the N phase was maintained till 2.5 wt% CDs but induced vertical alignment for the concentration (2.5 wt% $<$ conc. $\leqslant$ 5.0 wt%). However, the induced alignment remains vertical in the deep N phase and changes again to planar alignment with increase in temperature. This induced vertical alignment in the deep N phase is attributed to the higher pre-tilt angle ($\sim 8^{\circ}$) induced by CDs due to the macroscopic segregation of CDs to the planar anchored surfaces. A point to be noted here that (i) no induced vertical alignment in the SmA phase and (ii) induced homeotropic alignment in the deep N phase only (i.e. not thermally stable) by CDs (2.5 wt% $<$ conc. $\leqslant$ 5.0 wt%) are reported in this paper [59]. Our literature search (table 1, ESI) clearly reveals that there is no report on the induction of vertical alignment throughout the N and SmA phases of thermotropic smectogenic LC materials filled in planar anchored sample cells, by the dopant CDs (lowest concentration: 0.25 wt%). Henceforth, in this article, we report the induced vertical alignment in both the N and SmA phases of thermotropic smectogenic LC material, namely 8CB (4-octyl-4′-cyanobiphenyl) in planar anchored indium tin oxide (ITO) sample cells by dopant CDs, using an optical polarizing microscope and dielectric spectroscopic techniques. The detailed concentration and temperature-dependent optical, dielectric and electrical (i.e. conductivity) studies on CsD-8CB composites demonstrate significant changes in the molecular alignment and related dielectric and electrical properties. Most importantly, the observed results eventually support the achievement of thermally stable vertical alignment of 8CB, LC by dopant CDs, throughout both the N and SmA phases.

2. Experimental details

2.1. Materials

In the present study, as dopant we utilized organosoluble CDs ($\sim$7–8 nm), which were synthesized through a one-pot selective method [60], and characterized using various spectroscopic techniques such as Fourier transform infrared, transmission electron microscopy, thermogravimetric analysis, fluorescence confocal polarizing microscopy, etc, by the S Kumar group [61]. Afterwards, the chemical structure of these CDs and their formation mechanism were reported by Minervini *et al* [62]. A highly polar thermotropic smectogenic LC material, namely 8CB (4-octyl-4′-cyanobiphenyl) was procured from Sigma-Aldrich and utilized without any further purification. The host LC material (8CB) exhibits a phase sequence as follows: I (40.5 °C) N (32.5 °C) SmA (21.5 °C) Cr, wherein I, N, SmA and Cr denote isotropic, nematic, smectic A and crystalline phases, respectively. The chemical structures of 8CB and CDs are shown in figure 1. We initially dispersed the CDs in chloroform ($CHCl_3$) and a solution (0.1 w/v%) was prepared. The desired concentrations were subsequently added to the host LC material to acquire 0.03 wt%, 0.05 wt%, 0.1 wt%, 0.25 wt%, 0.3 wt% and 0.5 wt% concentration, respectively. In order to obtain a homogeneous mixture, composites of these concentrations were carefully ultrasonicated for 2 h. Thereafter, the chloroform evaporated by heating the composites at an elevated temperature (i.e. above the boiling point of chloroform, 61.2 °C) for 1 h. For the optical textures and dielectric investigations, the prepared CDs-8CB composites were filled at isotropic temperature into the 5 μm thick planar anchored ITO-coated sample cells (Instec, Inc., USA).

2.2. Characterization methods

The optical studies were performed using a polarizing optical microscope (CENSICO International 13809, India), equipped with an imaging camera (AmScope, FMA050). The temperature of the planar anchored ITO sample cells was maintained through a customized heat stage equipped with a temperature controller connected to a circulating water bath (Thermotech, AQS-WB-200, India) with a temperature accuracy of $\pm$0.5 °C. Dielectric measurements were conducted using an LCR meter (nF, ZM2376, Japan) in a frequency range of 100 Hz–5.5 MHz with an oscillating voltage of 300 mV.

3. Results and discussion

3.1. Textural (i.e. optical) studies

Figure 2 illustrates the cross-polarized optical textures of pure 8CB and CDs-8CB composites at $T = 28$ °C (SmA phase). Figure 2(a) depicts the uniform planar aligned SmA phase of pure 8CB as expected. In 0.03 wt% CDs-8CB composite, the quality of the planar alignment remains more or less the same compared to the pure 8CB sample (figure 2(b)). There is no

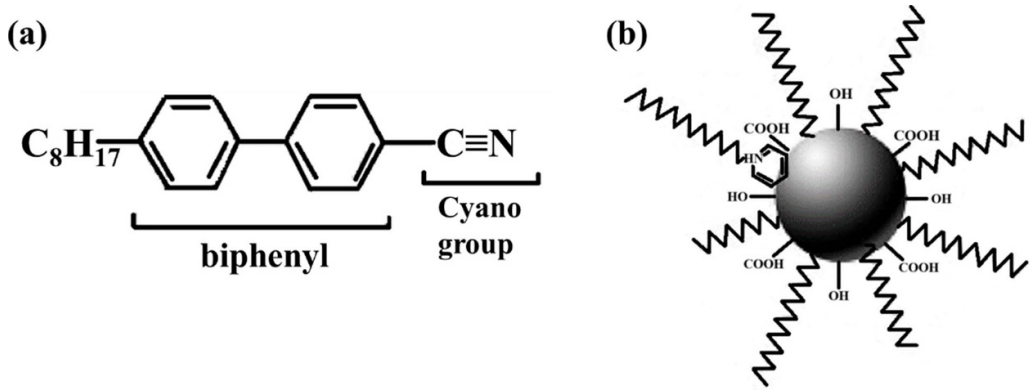

Figure 1. Chemical structure of (a) 8CB (4-octyl-4′-cyanobiphenyl) and (b) schematic of organosoluble CD. Adapted from [60] with permission from the Royal Society of Chemistry.

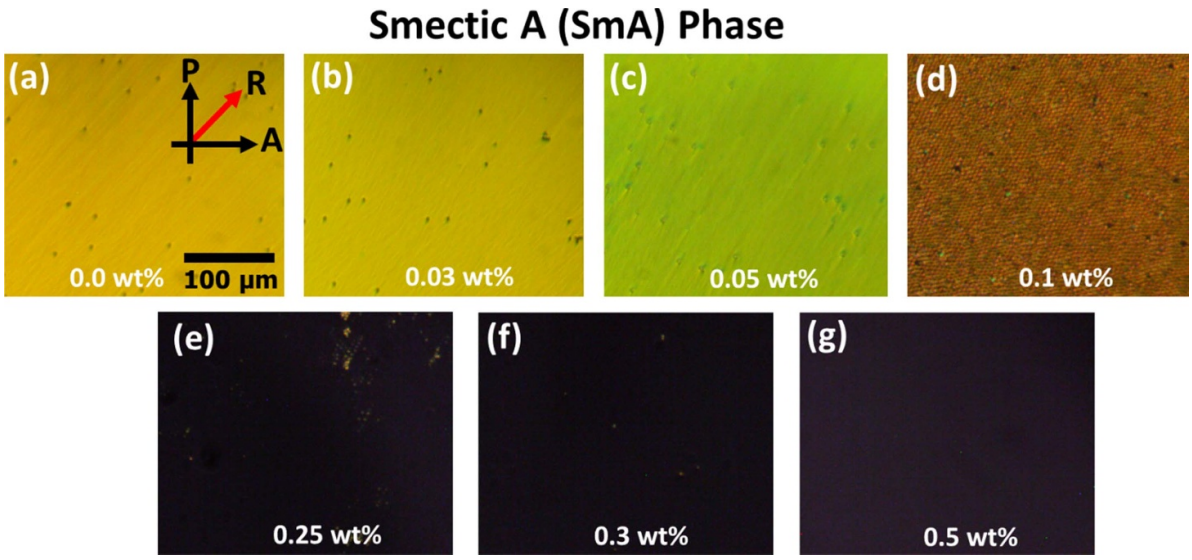

Figure 2. Optical micrographs of SmA phase (28 °C) of (a) 0.0 wt%, (b) 0.03 wt%, (c) 0.05 wt%, (d) 0.1 wt%, (e) 0.25 wt%, (f) 0.3 wt% and (g) 0.5 wt% of CDs-8CB composites. Here, P and A denote the polarizer and analyzer of the crossed polarized microscope, respectively, and R shows the rubbing direction. Scale bar is 100 μm. Optical textures shown in (a)–(c) and (e)–(g) demonstrate the planar and vertical alignments of the SmA phase of CDs-8CB composites, respectively. Optical texture shown in (d) shows the distorted planar alignment of 0.1 wt% composite.

significant change in the uniformity of the planar alignment of SmA of the 0.05 wt% CDs-8CB composite (figure 2(c)) compared to the 0.03 wt% composite and pure 8CB sample, except for the color change. This change in color could be attributed to the change in the refractive index of the composites due to the presence of CDs. However, further increase in the concentration to 0.1 wt% led to the degradation in alignment of the composite, as can be seen in figure 2(d). It eventually shows a distorted texture which gives an indication of the effect of CDs on the alignment layer (planar anchored) of the LC cell. Surprisingly, 0.25 wt% CDs are able to induce a vertical alignment of the LC molecules in the SmA phase of 8CB (figure 2(e)). Nevertheless, a focused observation clearly indicates that some inhomogeneity is still edging its way into the optical texture, indicating that a complete dark state is yet to be achieved. However, figures 2(f) and (g) exhibit a uniform dark texture for 0.3 wt% and 0.5 wt% CDs-8CB composites indicating the effect of CDs on the 8CB material. A striking feature of this observation is the tunability of SmA alignment by CDs and its ability to change the pre-existing planar alignment to the vertical state at such a low concentration in the SmA phase of 8CB, LC.

Similarly, the effect of CDs on the alignment of the N phase (38 °C) in the planar anchored sample cells is shown in figure 3. As can be seen from this figure, the planar alignment of the N phases in 0.03 wt% and 0.05 wt% CDs-8CB composites remains more or less the same as pure 8CB (figures 3(a)–(c)). The alignment of the N phase in 0.1 wt% CDs-8CB composite is distorted compared to that in the pure 8CB and composites up to 0.05 wt% CDs and attributed to the strong interaction of the CDs with the planar anchored ITO substrate (figure 3(d)). However, the induction of vertical alignment in the N phase after doping of 0.25 wt% CDs is obtained (figure 3(e)). Interestingly, a more uniform vertical alignment of the N phase is produced for 0.3 wt% and 0.5 wt% CDs-8CB composites (figures 3(f) and (g)) as it was in the case of

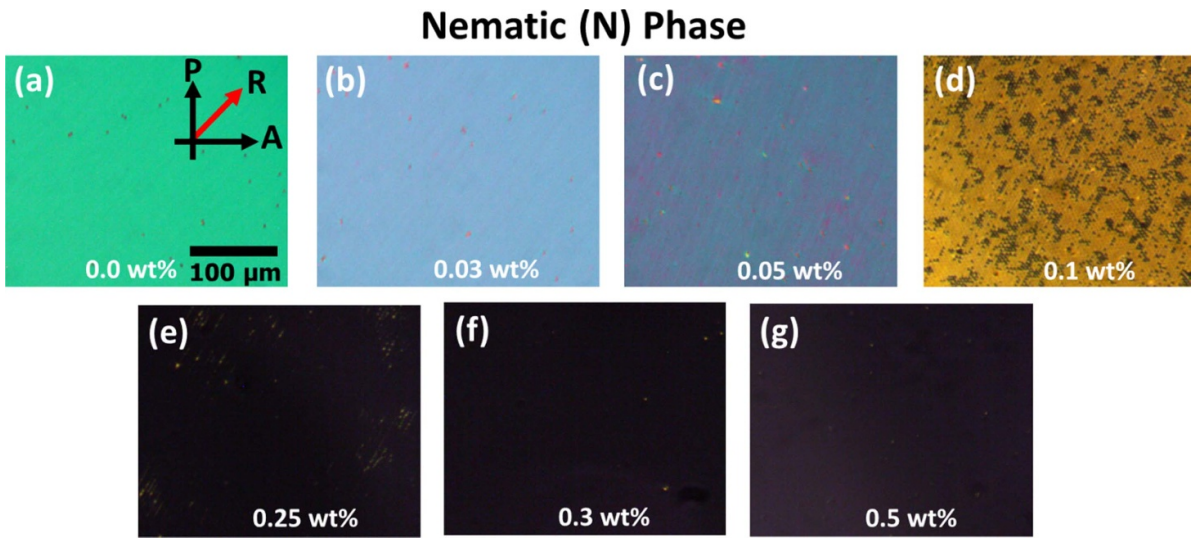

Figure 3. Optical micrographs of the N phase (38 °C) of (a) pure 8CB, (b) 0.03 wt%, (c) 0.05 wt%, (d) 0.1 wt%, (e) 0.25 wt% (f) 0.3 wt% and (g) 0.5 wt% of CDs-8CB composites. Here, P and A denote the polarizer and analyzer of the crossed polarized microscope, respectively, and R shows the rubbing direction. Scale bar is 100 μm. Optical textures shown in (a)–(c) and (e)–(g) demonstrate the planar and vertical alignments of the N phase of CDs-8CB composites, respectively. Optical texture shown in (d) shows the distorted planar alignment of 0.1 wt% composite.

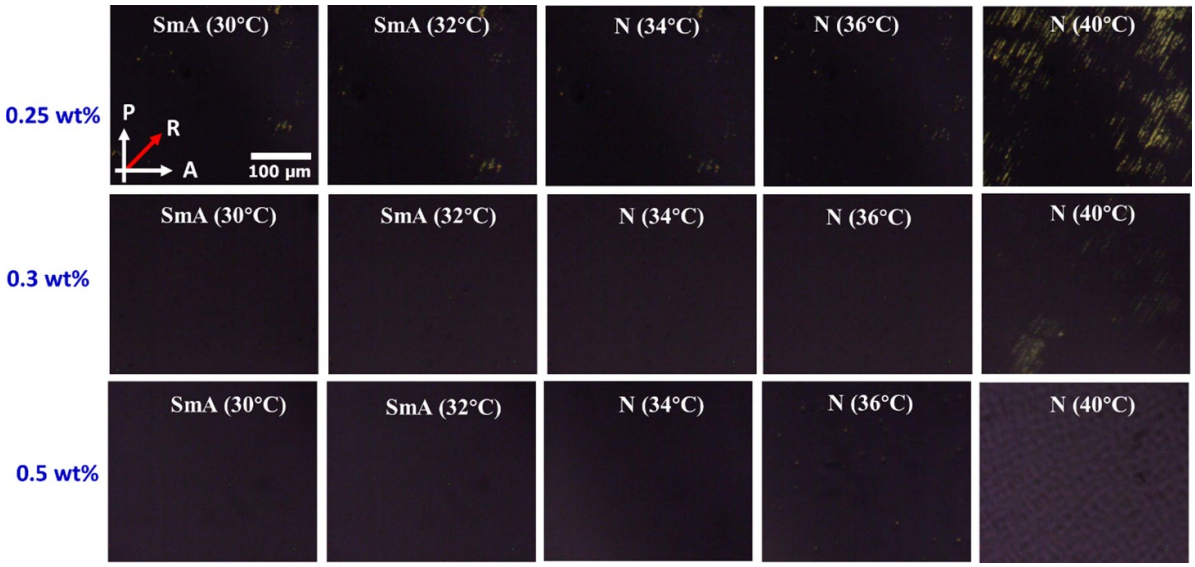

Figure 4. Temperature-dependent cross-polarised optical micrographs of both SmA and N phases of vertical aligned CDs-8CB composites (CD concentration: 0.25 wt% , 0.3 wt% and 0.5 wt%). Here, P and A denote the polarizer and analyzer of the crossed polarized microscope, respectively, and R shows the rubbing direction. Scale bar is 100 μm.

CDs-8CB composites [54]. We anticipate that the adsorption of CDs on the planar anchored ITO-coated substrates plays an important role in tuning the alignment of the 8CB molecules. For instance, in the case of lower concentrations of CDs, the anchoring force produced by the alignment layer predominates the interaction of CDs with the substrate illustrating a uniform planar alignment in the optical texture. Nevertheless, an increase in the concentration of CDs eventually produces a stronger interaction of these dots with the substrate surface, leading to the obliteration of the pre-existing planar alignment of the 8CB molecules.

After the confirmation of the induced vertical alignment of 8CB molecules in both the SmA and N phases (at one temperature point), it is worth checking their stability throughout both LC phases. Therefore, we have recorded the cross-polarized optical textures of 0.25 wt%, 0.3 wt% and 0.5 wt% CDs-8CB composites throughout the SmA and N phases, as shown in figure 4.

Obviously, the induced vertical alignment remains stable throughout the LC phases of 8CB that eventually indicates its thermal stability (figure 4). It is worth pointing out here that some light streaks can be observed in 0.25 wt% CDs-8CB composites. However, 0.3 wt% and 0.5 wt% CDs-8CB composites show the perfect dark state with almost no light leakage as the composite transits from one phase to another. To the best of our knowledge, such a remarkable thermally

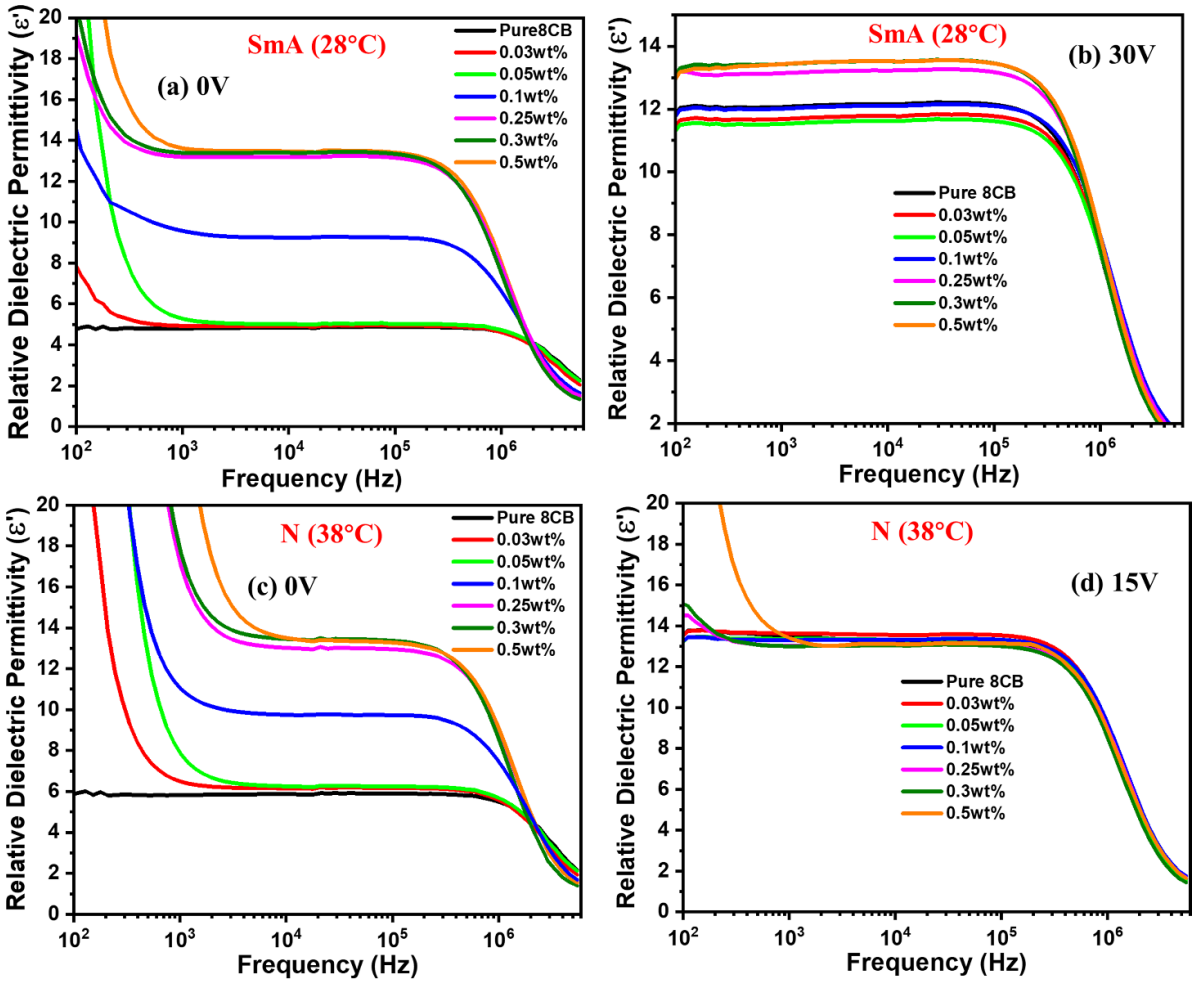

Figure 5. Frequency-dependent relative dielectric permittivity (ε') of pure 8CB and CDs-8CB composites for (a) 0 V and (b) 30 V at 28 °C (SmA), and (c) 0 V and (d) 15 V at 38 °C (N), respectively.

stable induced vertical alignment throughout the SmA and N phases of 8CB using CDs has not been reported so far. By using optical textures of pure 8CB, the transition temperatures of SmA-N ($T_{\text{SmA-N}}$) and N-Iso ($T_{\text{N-I}}$) were found to be 33.5 °C and 41 °C, respectively. From the analysis of the temperature-dependent optical textures (figure 4) it was concluded that no change occurred in $T_{\text{SmA-N}}$ for these composites (0.25 wt%, 0.3 wt% and 0.5 wt%) exhibiting induced vertical alignment. $T_{\text{N-I}}$ was also found to remain invariable for the 0.25 wt% and 0.3 wt% composites. However, for 0.5 wt% there was a decrease in $T_{\text{N-I}}$ by ∼1 °C compared to pure 8CB.

3.2. Dielectric studies

Frequency-dependent dielectric spectroscopy is another versatile technique to confirm the molecular alignment of LC materials and their nanocomposites since it probes the molecular dynamics [63–67]. We have employed this technique to investigate the impact of CDs on various dielectric features such as permittivity, loss, and relaxation of both SmA and N phases of LC (8CB) material. The frequency-dependent relative dielectric permittivity (ε') for various concentrations of CDs in the SmA (T = 28 °C) and N (T = 38 °C) phases of 8CB is shown in figure 5.

As can be seen from figure 5(a) at 0 V that the value of ε' increases dramatically with an increase in dopant concentration. For lower concentration, such as 0.03 wt% and 0.05 wt%, ε' did not show much variation compared to pure 8CB. However, a substantial increase in ε' was observed for the composites with concentration ⩾0.1 wt%. The composites that attained vertical alignment (⩾0.25 wt%) illustrated overlapping values (figure 5(a)). These values remained more or less similar to the ones achieved after the application of 30 V (figure 5(b)), confirming the induced vertical alignment. This is the lowest concentration (0.25 wt%) ever reported that could induce vertical alignment in the SmA phase by CDs, QDs and nanorods/nanoclusters/NPs (table 1, ESI). It is worth pointing out here that in comparison to the N phase, the higher ordering of the SmA phase caused by its layered structure makes it more challenging to align it vertically. Nevertheless, we may speculate that even in 0.25 wt% composite, the very strong interaction of CDs with planar anchored ITO substrates than LC molecules fosters vertical alignment of LC molecules, which eventually led to orient smectic layers parallel to the substrates from the perpendicular direction. The induction of vertical alignment in our study is attributed to the QD (in our case CD) accumulation at the substrate surface, which has been illustrated using schematic

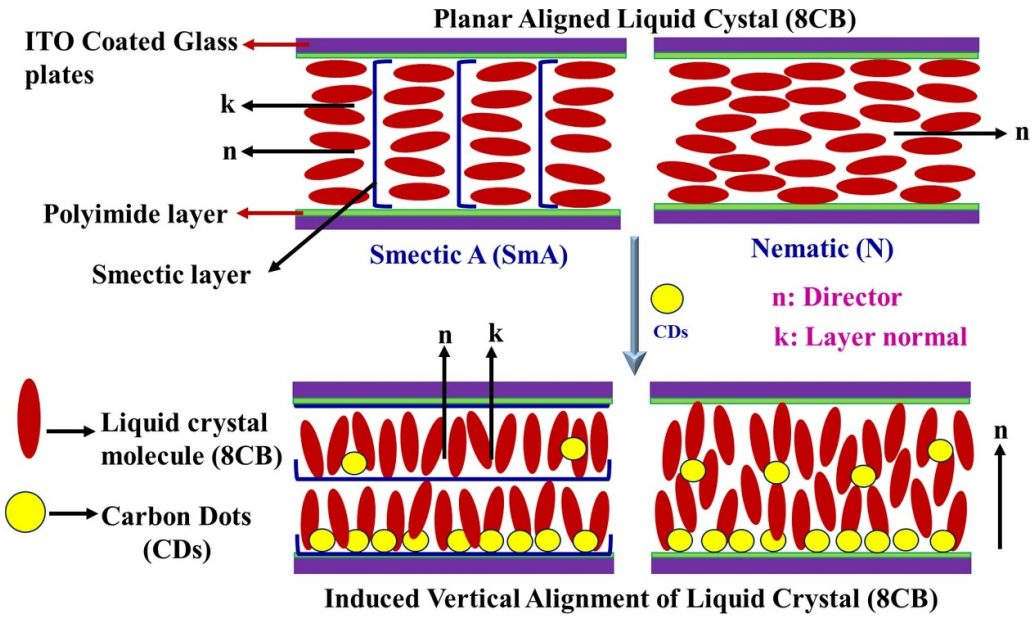

Figure 6. Schematic of planar and induced vertical alignment of SmA and N phases of LC, 8CB and CDs-8CB composites in planar anchored ITO sample cells, respectively. For clarity, the dimensions of LC molecules and CDs are not to scale. Smectic layers are parallel and perpendicular to the ITO-coated glass substrates in planar and vertically aligned sample cells, respectively. Reorientation of director (**n**) in both SmA and N phases from planar to vertical alignment geometries is done by the dopant CDs and not by an external electric field.

representation in figure 6. The propensity of QDs to accumulate at the substrate surfaces alters the existing alignment by weakening the surface anchoring energy of the substrates. The ejection of QDs from the nematic phase causes them to accumulate at the substrate surface, eventually providing a robust coverage on the initial alignment layer of the cell [68, 69]. For a variety of reasons, the interaction at the surface is possibly a better alternative because, first of all, surface interactions produce a stronger force initially causing the LC molecules at the interfaces to produce a pretilt, thereafter orienting the molecules in the bulk to follow the direction indicated by the surface molecules [70]. Second, accumulation of QDs at the interfaces does not degrade the texture in the bulk with concentration up to a certain level. This accumulation of QDs at the interfaces can help in eliminating the use of alignment layers in conventional LC-based devices [32]. Application of 30 V was able to reorient the molecules to the vertical state for pure 8CB at $T = 28$ °C (figure 5(b)). Nevertheless, for lower concentrations (0.03 wt% and 0.05 wt%) the value of the permittivity was observed to be lower than for pure 8CB. For 0.1 wt% composite, the value was overlapping with pure 8CB, but for concentration $\geqslant$0.25 wt% exhibited a better dark state, as illustrated through the higher permittivity value, which corroborates well with the optical texture observed (figure 2). Investigating the dielectric permittivity at the N phase ($T = 38$ °C) revealed the consistency of this vertical alignment with changing temperature (figure 5(c)). The increase in the permittivity of the N phase for pure 8CB and composites with lower concentrations is attributed to the phase change from SmA to N. At higher concentration ($\geqslant$0.25 wt%), the increased value of permittivity exhibits the persistent vertical alignment with varying phase. This turns out to be the most intriguing phenomenon since such consistency in the vertical alignment during phase change has not been seen before at CD concentration (0.25 wt%). Then, 15 V was applied in the N phase to examine whether the quality of the vertical alignment produced in pure 8CB corroborates with composites showing induced vertical alignment (figure 5(d)). It can be seen that there is basically no significant difference in the value of permittivity after applying the voltage for concentrations $\geqslant$0.25 wt%. However, it was observed that the application of voltage was able to reduce the ionic factor profoundly in almost all concentrations, except for 0.5 wt% (figures 5(b) and (d)).

Figure 7 illustrates the variation in dielectric loss (ε'') with and without the application of an external bias field. When no bias field is applied in the SmA phase of 8CB LC, as shown in figure 7(a), one can observe the appearance of short axis molecular relaxation in the composites, in which vertical alignment is induced by CDs ($\geqslant$0.25 wt%). Here, 0.1 wt% composite also tries to exhibit a weaker short axis molecular relaxation, being the intermediate state. However, the lower concentrations do not exhibit such relaxation and behave monotonously as pure 8CB. Figure 7(b) shows that a 30 V external DC bias was applied to change the orientation of pure 8CB and composites with lower concentrations from planar to vertical state, thereby giving rise to short axis molecular relaxation. Application of an external bias field on the composites having induced vertical alignment did not cause any significant change, neither on the width nor on the height of the short axis molecular relaxation peak and eventually gave a clear indication of the perfect dark state exhibited by the CDs-8CB composites due to the surface interactive property [54]. The variation in ε'' was also checked in the N

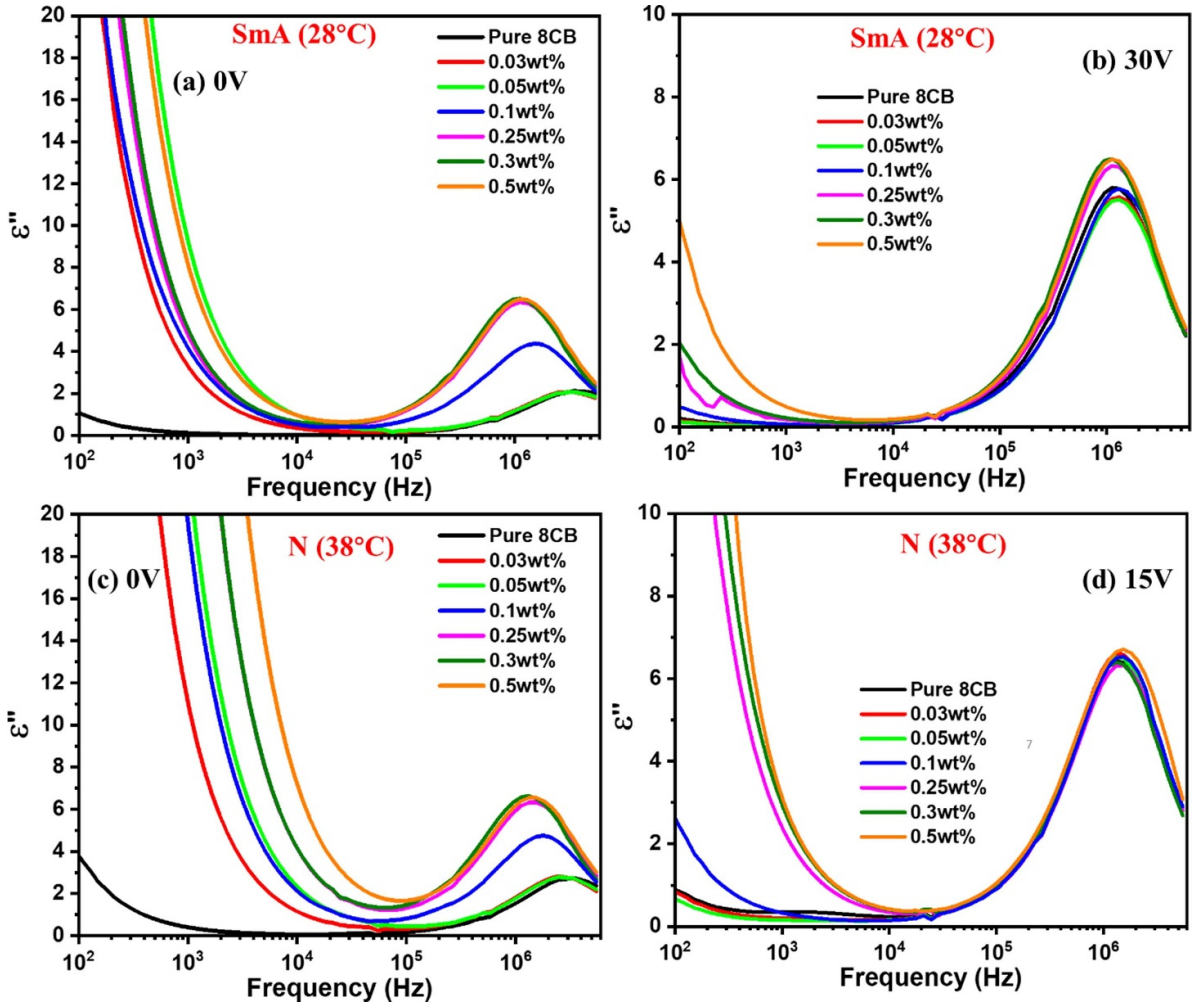

Figure 7. Frequency-dependent dielectric loss (ε'') of pure 8CB and CDs-8CB composites for (a) 0 V (b) 30 V at 28 °C (SmA) and (c) 0 V (d) 15 V at 38 °C (N).

phase of 8CB LC, as demonstrated in figures 7(c) and (d). In the absence of an external field (figure 7(c)), ε'' exhibited a striking similarity to that seen in the SmA phase. Short axis molecular relaxation was also observed for composites exhibiting induced vertical alignment even in the N phase, confirming the thermal stability of the alignment as the sample was heated to the N phase from the SmA phase. Here, a 15 V DC bias was applied to pure 8CB and composites and it was again confirmed that the CDs were able to induce a perfect vertical state since no change was observed in the relaxation peak before and after the application of external bias in the composites having induced vertical alignment (figure 7(d)). Concentration-dependent variation in short axis relaxation frequency is shown in figure S1.

Concentration-dependent study gives us an overview of the relative increment in the value of ε' for composites with varying concentration. Here, figure 8(a) illustrates the value of permittivity for pure 8CB at 0 V to be 4.84 and 12.15 at 30 V in the SmA phase. However, for composite $\geqslant$0.25wt% this difference reduces drastically exhibiting coinciding values. These coinciding values confirm the induced vertical alignment of SmA produced by CDs. A similar scenario can also be observed in the N phase (figure 8(b)) wherein the comparable values of ε' at 0 and 15 V for composite $\geqslant$0.25wt% confirms the induced vertical alignment.

The temperature-dependent variation in ε' of the pure 8CB and CDs-8CB composites throughout the SmA to N phases is shown in figure 9. It illustrates a marginal increase in the value of permittivity when the sample goes to N phase, which could be attributed to the lowering of rotational viscosity. The value of ε' in composites exhibiting vertical alignment ($\geqslant$0.25wt%) remains invariant with changing temperature. Through dielectric measurements, the SmA-N transition temperature ($T_{\text{SmA-N}}$) is found to be 34 °C and the N-Isotropic temperature ($T_{\text{N-I}}$) is found to be 41 °C. No shift occurred in the $T_{\text{SmA-N}}$ for all CDs-8CB composites compared to pure 8CB. Similarly, most CDs-8CB composites showed no variation in $T_{\text{N-I}}$ except for 0.5wt% composite, which exhibited $\sim$1 °C decrease compared to pure 8CB.

3.3. *Electrical (conductivity) studies*

The loosely bound charged particles exhibit mobility in response to an external stimulus that is subsequently responsible for the material's apparent conductivity (σ). The movement of the charged particles and their reaction towards

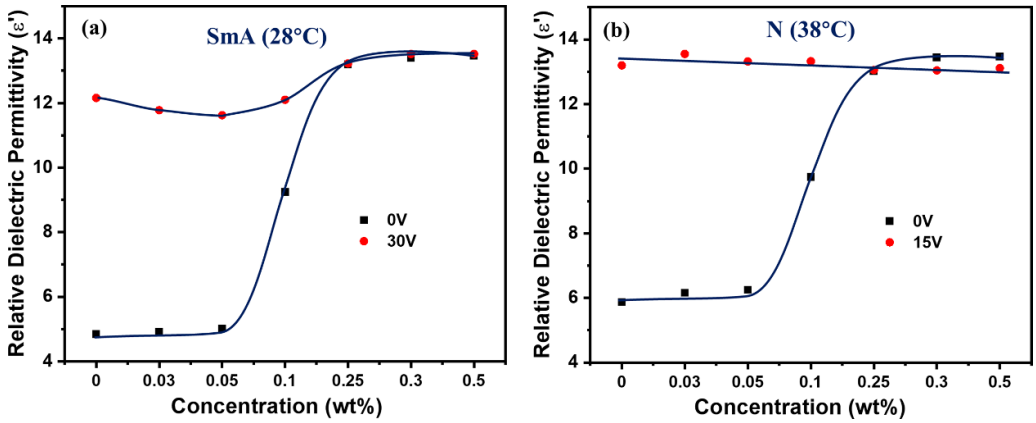

Figure 8. Concentration-dependent relative dielectric permittivity (ε') at a constant frequency of 10 kHz for (a) SmA and (b) N phases of pure 8CB and CDs-8CB composites.

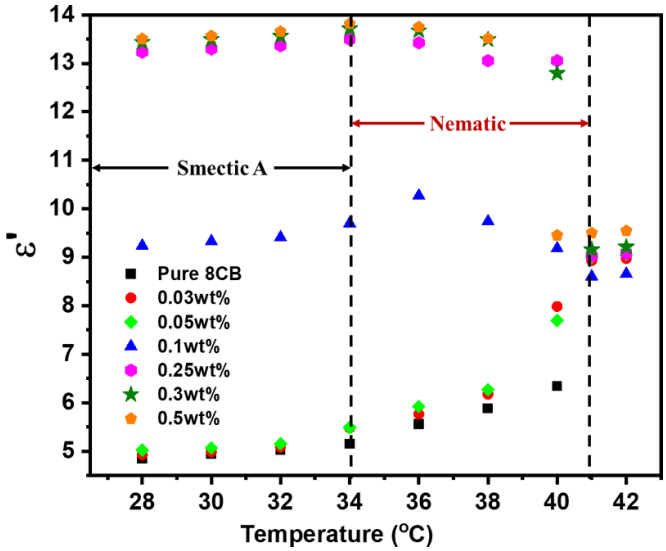

Figure 9. Temperature-dependent relative dielectric permittivity (ε') of pure 8CB and CDs-8CB composites at a constant frequency of 10 kHz.

temperature and frequency affects the material's electrical response [71]. Figure 10 demonstrates the variation in σ as a function of angular frequency (ω) in the SmA and N phases for pure 8CB and CDs-8CB composites. Here, we have calculated σ using the general relation:

$$\sigma = 2\pi f \varepsilon_o \varepsilon'', \tag{1}$$

whereby ε_0 denotes the permittivity of free space, i.e. $8.854 \times 10^{-12}\,\mathrm{m^{-3}\,kg^{-1}\,s^4\,A^2}$, and ε'' denotes dielectric loss of the medium. The plot figure 10(a) shows a dramatic increase in conductivity with the addition of CDs in host 8CB LC. The plot shows three different regions for composites that are categorized as low, mid and high. The low region (10^1–10^2 Hz) corresponds to reduced σ that occurs as a result of an electrode polarization effect since the addition of CDs produces enhanced conductivity due to the increase in ions, and subsequently these ions try to accumulate at the sample electrode interface, thus decreasing the conductivity. The mid region (10^2–10^4 Hz) is a plateau that corresponds to frequency-independent DC conductivity and the high region ($\geqslant 10^5$ Hz), which exhibits a sharp increase in conductivity with frequency is accredited to the AC conductivity [72]. Since the frequency-dependent conductivity apparently follows Jonscher's universal dynamic response [73], total conductivity ($\sigma(\omega)$) is represented as:

$$\sigma(\omega) = \sigma_{\mathrm{dc}} + A\omega^n, \tag{2}$$

where σ_{dc} corresponds to DC conductivity, A denotes the pre-exponential constant, $\omega = 2\pi f$ is the angular frequency and n denotes the power-law exponent ($0 < n < 1$). The exponent value 'n' expresses the interplay between mobile ions and their surrounding lattice and was observed to be beyond Jonscher's limit for all samples under analysis. The dipolar part can be overlooked for the low-frequency region; thereby $\sigma(\omega) = \sigma_{\mathrm{dc}}$. From the fitted data (figure 10(a)), the value of σ_{dc} for pure 8CB is observed to be 5.96×10^{-9}, and for composites it exhibits an increase of up to two orders of magnitude in that

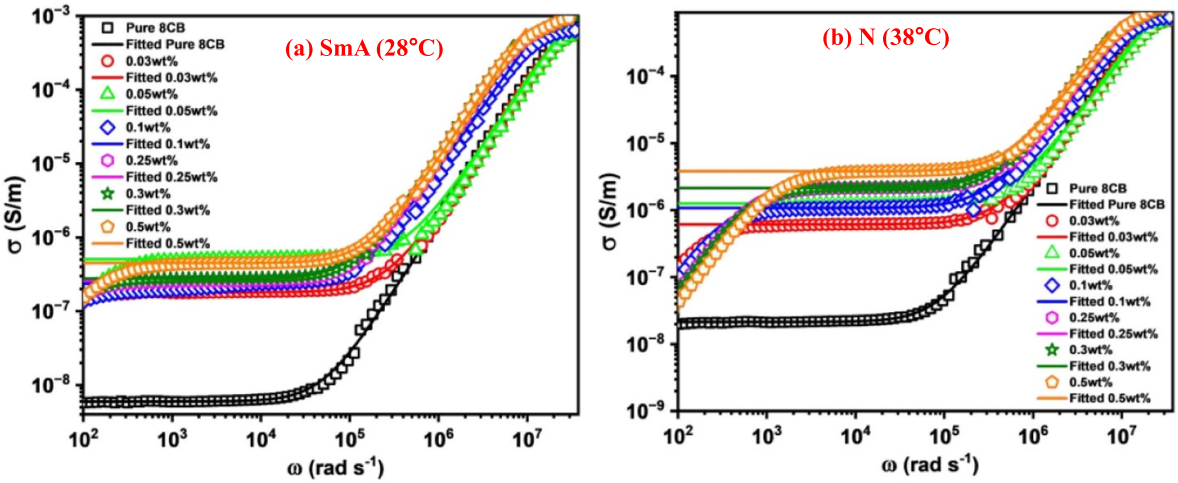

Figure 10. Angular frequency (ω) dependent conductivity (σ) at (a) the SmA and (b) N phase of pure 8CB and CDs-8CB composites and fitted with Jonscher's power law (JPL). Symbols and solid lines represent the experimental data and JPL fitting curves, respectively.

0.05 wt% shows the highest value, i.e. 5.0828×10^{-7}. For lower concentrations σ_{dc} remains more prominent because at higher concentrations, the drifting of charge carriers imposes hurdles in the mobility of ions [74], thereby also exhibiting increased activation energy (figure 3(a)). However, in this study, at higher concentration ($\geqslant$0.25 wt%) a change in alignment of composites occurs from planar to vertical facilitating the flow of ions, thus demonstrating increments in conductivity values. Analyzing the conductivity trend in the N phase in figure 10(b) the value of σ_{dc} for pure 8CB is 2.15×10^{-8} and for 0.5 wt% it increases to 3.8×10^{-6}, an enhancement of up to two orders, again similar to the SmA phase. However, in the N phase with increasing concentration σ_{dc} is observed to rise significantly, which can be attributed to the lower ordering of the N phase since in less viscous medium ions tend to be more mobile. The ionic impurities that are initially bound with the CDs get detached, at least partially, when interacting with 8CB and attain a uniform dispersion in the medium. Since 8CB is a highly polar material, its cyano group facilitates the dissolution of ions, thereby increasing the conductivity with increasing concentration of CDs [74].

Since vertical alignment more effectively facilitates the flow of mobile ions compared to its planar counterpart, the increment in their σ_{dc} value remains higher. A similar trend was observed in our previous study with 5CB where an enhancement of $\sim$18 times in σ_{dc} was observed in the sample that exhibited vertical alignment with the doping of CDs [55]. The electrode polarization effect in the low-frequency region saw a huge shift towards the higher frequency side with increasing concentration, which would be accredited to the accumulation of ions at the electrode interface due to (i) the addition of ions with increasing concentration and (ii) the thin sample cell that is used for the investigation [74, 75].

The variation of the logarithmic dc conductivity with absolute temperature fitted using the Arrhenius equation [71] is given as:

$$\ln(\sigma_{dc}) = \ln(\sigma_o) - \frac{E_a}{k_b T}, \tag{3}$$

where E_a represents the activation energy, σ_o is the pre-exponential factor, T denotes the temperature and k_b is the Boltzmann constant. From figure 11, conductivity is observed to increase linearly with increasing temperature in both SmA and N phases for all samples. In the SmA phase, the value of σ_{dc} remains relatively low. Nevertheless, after the transition to the N phase a significant increase in the value of σ_{dc} occurs due to the lowering of viscosity with increasing temperature. Lowered viscosity eases the mobility of ions in the medium, thereby increasing the conductivity. For lower concentrations ($\leqslant$0.1 wt%), the rise in σ_{dc} with temperature exhibits a linear increase. However, for 0.05 wt% at 28 °C, σ_{dc} is highest but with increasing temperature it does not retain the highest value. The activation energy (E_a) for 0.05 wt% was observed to be the lowest out of all samples under investigation (figure 3). In the N phase, due to the enormous rise in σ_{dc} for higher concentrations ($\geqslant$0.25 wt%), 0.05 wt% follows a usual trend. The rise in σ_{dc} for pure 8CB from SmA to N is $\sim$3.6 times, which increases to 8.5 times in 0.5 wt% composite. However, for 0.05 wt%, a marginal increase of only 2.5 times occurs, thereby eliminating the anomaly observed in the SmA phase. In the N phase, 0.5 wt% shows the highest value of σ_{dc} throughout the temperature range of 8CB LC due to the induction of vertical alignment. Concentration-dependent activation energy (E_a) in the SmA and N phases of pure 8CB and CDs-8CB composite is shown in figure S3.

3.4. Voltage-dependent dielectric and optical studies

3.4.1. Dielectric study. In this section, we discuss the effect of varying voltage on the dielectric permittivity of the SmA (28 °C) and N (38 °C) phases of pure 8CB and CDs-8CB composites, shown in figures 12 and 13, respectively.

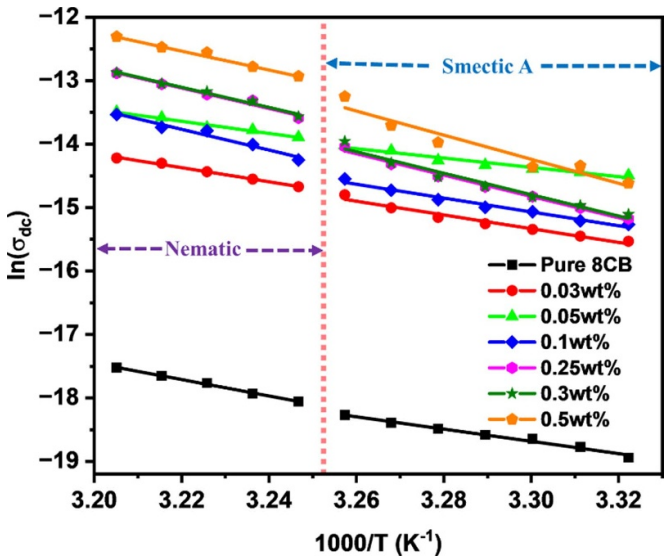

Figure 11. Variation in $\ln(\sigma_{dc})$ with the inverse of absolute temperature in the SmA and N phases of pure 8CB and CDs-8CB composites (fitted Arrhenius plot). R^2 varies from 95%–99%. Experimental data are represented using symbols, and solid lines indicate the fitting with the Arrhenius equation.

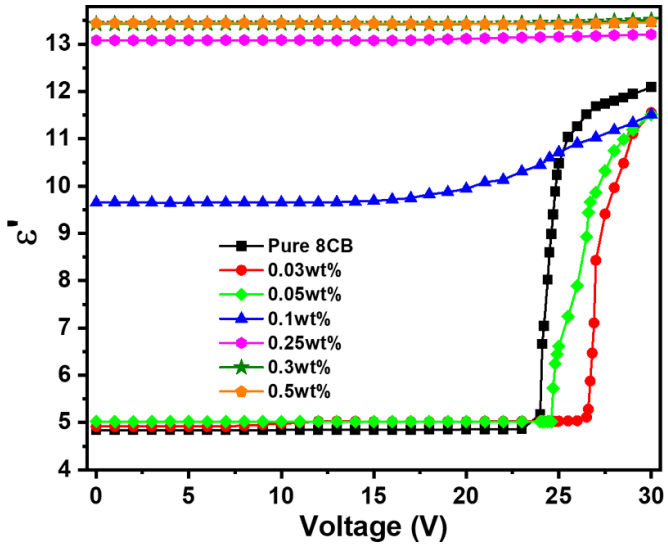

Figure 12. Voltage-dependent relative dielectric permittivity (ε') for the SmA phase ($T = 28$ °C) of pure 8CB and CDs-8CB composites at a constant frequency of 10 kHz.

Since SmA is a higher-ordered phase than N phase, a maximum of 30 V was applied to switch the planar aligned composites into the vertical state, as shown in figure 12. The threshold voltage (V_{th}) for pure 8CB was observed to be 24 V, which was further increased to 26.7 V for the lowest composite 0.03 wt%. However, for 0.05 wt%, V_{th} was decreased and found to be 24.7 V, whereafter a further increase in concentration to 0.1 wt% exhibited relatively no threshold, except for a slight increase in the value of ε' demonstrated by a curved line. Composites ($\geqslant$0.25 wt%) demonstrated absolutely no change in ε' value with increasing voltage. This illustrates that vertical alignment induced by CDs produces a perfect dark state,

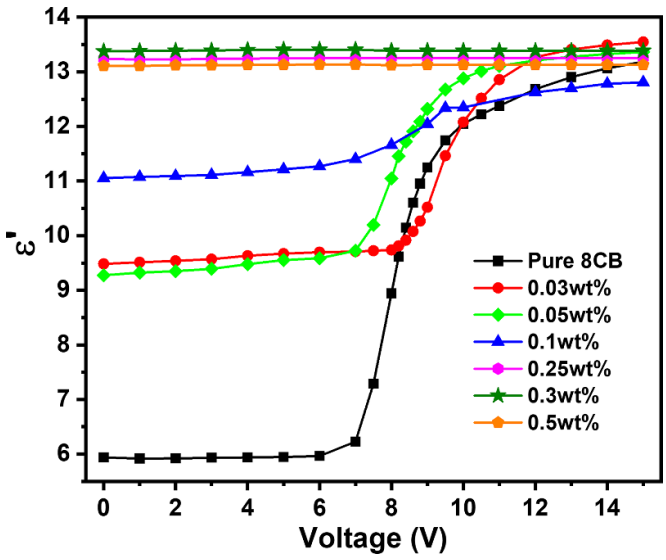

Figure 13. Voltage-dependent relative dielectric permittivity (ε') for the N phase ($T = 38$ °C) of pure 8CB and CDs-8CB composites at a constant frequency of 10 kHz.

leaving no more scope for any changes in alignment of 8CB molecules. This can again be attributed to the direct interaction of CDs with the planar anchored substrate surface.

For the N phase (figure 13), voltage-dependent ε' produced a similar trend to that observed in the SmA phase. For instance, the V_{th} observed for pure 8CB was 7.1 V, which further increased to 9 V for 0.03 wt%. However, for 0.05 wt% the value reduced to 7.5 V. For the composites that exhibited an induced vertical alignment ($\geqslant$0.25 wt%), it was observed that the external electric field produced no variation, validating the perfect dark state also having being induced by CDs in the N phase. It should be noted here that the ε' value in the N phase (external field of 30 V was applied in the SmA phase and then heated to the N phase after removal of 30 V in SmA) in composites (0.03 wt% and 0.05 wt%) at 0 V is larger than the value when no electric field was applied in the SmA phase (figure S2).

3.4.2. Optical study. We have also investigated the effect of voltage on cross-polarized optical textures of pure 8CB and CDs-8CB composites at 28 °C (SmA) and observed that the application of $V > V_{th}$ produces changes in the planar texture of pure 8CB and other lower concentration composites, as shown in figure 14. For $V < V_{th}$, no change was observed in the optical texture, correlating with the voltage-dependent permittivity graph shown in figure 12. However, composites ($\geqslant$0.25 wt%) show no variation in optical texture with voltage, validating the perfect vertical state induced by CDs.

In figure 15, a maximum of 15 V was applied unlike in SmA, due to the lower ordering present in the N phase, which makes them easier to reorient even at lower voltages. The optical textures of pure 8CB and composites with lower concentrations exhibited a variation with voltage and attained a vertical state at 15 V. As can be observed in planar aligned composites ($<$0.1 wt%), the optical texture remains uniform (0

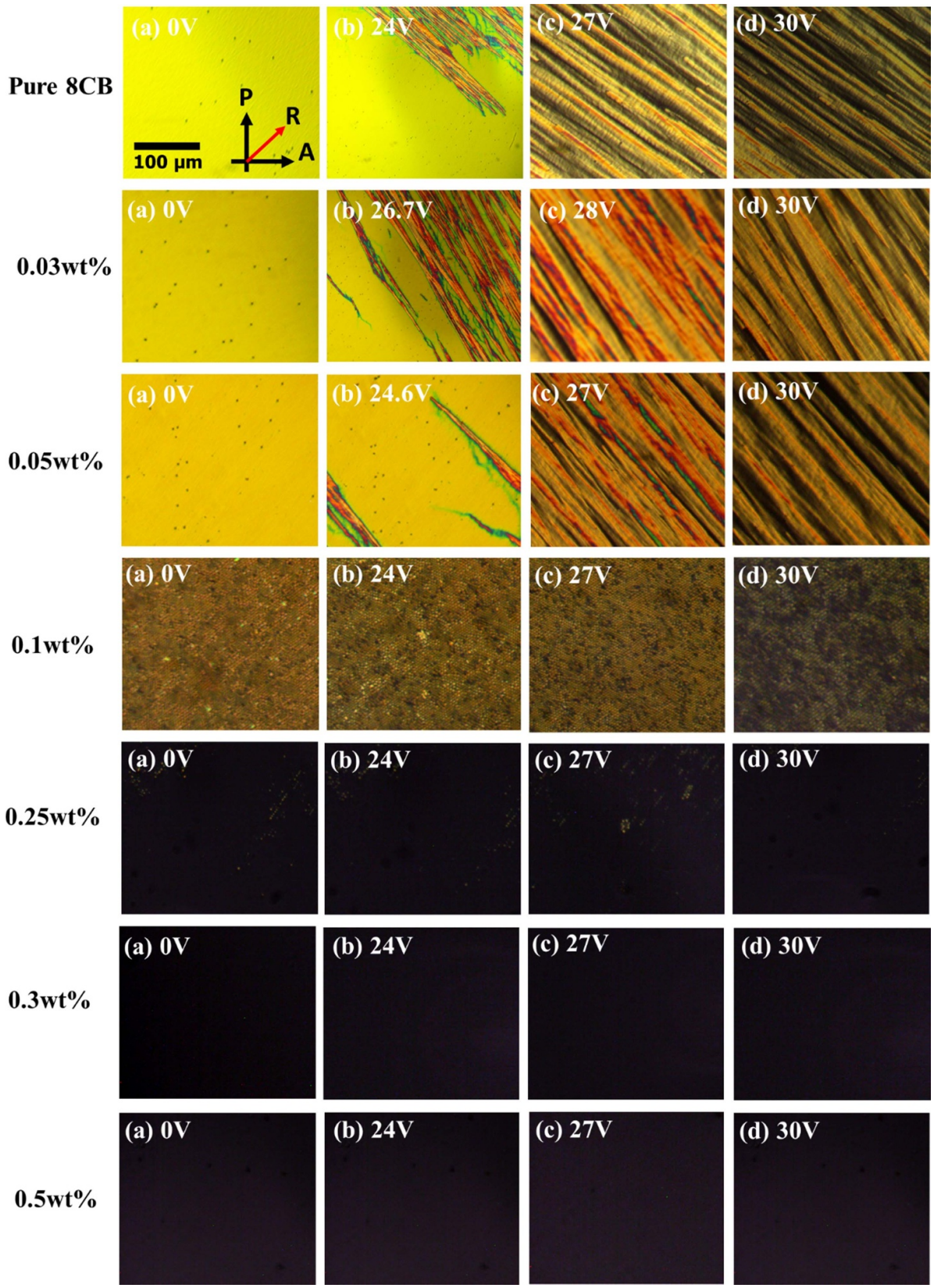

Figure 14. Voltage-dependent optical textures for pure 8CB and CDs-8CB composites at 28 °C (SmA). Here, P and A denote the polarizer and analyzer of the crossed polarized microscope, respectively, and R shows the rubbing direction. Scale bar is 100 μm.

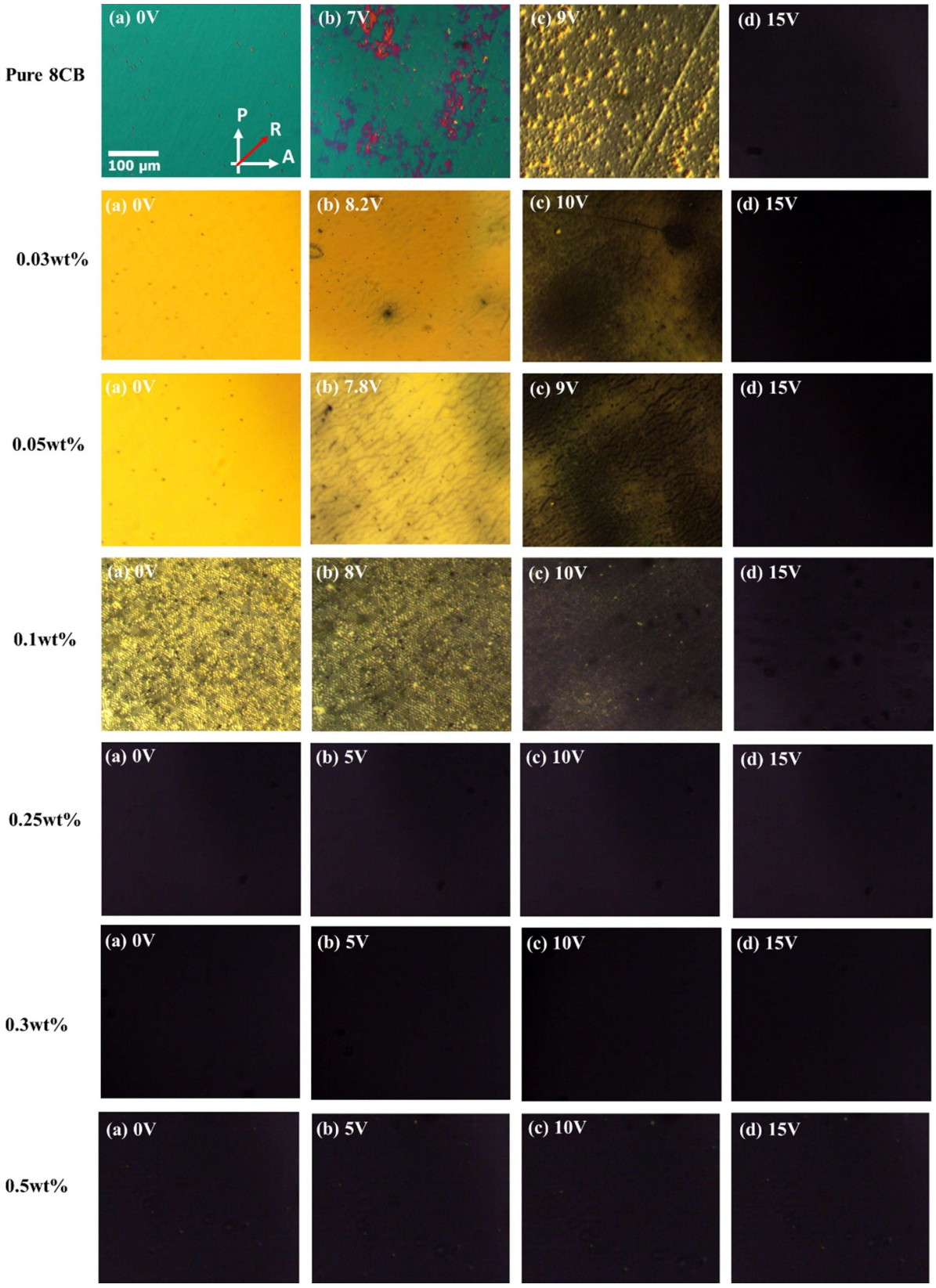

Figure 15. Voltage-dependent optical micrographs of pure 8CB and CDs-8CB composites at 38 °C (N phase). Here, P and A denote the polarizer and analyzer of the crossed polarized microscope, respectively, and R shows the rubbing direction. Scale bar is 100 μm.

and 5 V) till it reaches V_{th}. However, changes can be observed happening in the optical texture and eventually reaching a complete dark state (15 V). Composites exhibiting vertical alignment illustrated no change in the texture corroborating well with the dielectric data shown in figure 13.

4. Conclusion

We prepared CDs-doped 8CB composites and demonstrated the changes in molecular alignment, dielectric and electrical properties throughout the SmA and N phases of CDs-8CB composites infiltrated into planar anchored ITO sample cells by using a cross-polarized optical microscope and frequency-dependent dielectric spectroscopy. The cross-polarized optical textures of the composites confirmed the impact of CDs on the molecular alignment of the host LC material, and a vertical alignment was induced for concentration $\geqslant$0.25 wt% in both the SmA and N phases of CDs-8CB composites. Moreover, the value of the real dielectric permittivity (ε') was also found to gradually increase with concentration and provided analogous values of permittivity (conc.$\geqslant$ 0.25 wt%) with and without bias field, and the presence of short axis molecular relaxation at 0 V for composites $\geqslant$0.25 wt% in both SmA and N phases provided confirmation of the induced vertical alignment. Interestingly, this is the lowest concentration of CDs (0.25 wt%) required to induce such a strong vertical alignment in the SmA phase of 8CB LC without application of any external electric field. It is worth pointing out here that composites exhibiting vertical alignment in the SmA phase induced by CDs are substantially better than the alignment generated through an external electric field. However, in the N phase, the alignment produced by the former and latter remains analogously identical. Moreover, a rise in the value of conductivity occurred due to the doping of CDs, which became enhanced as the composites moved from the SmA to the N phase for all samples under analysis. We anticipate that the accumulation of CDs at the surface of planar anchored ITO substrates could be attributed as an important factor for this change in alignment as well as dielectric and electrical parameters. Most importantly, the doping of CDs in smectogenic 8CB LC is capable of producing a perfect dark state throughout the N and SmA phases. Undoubtedly, these CDs-8CB composites could certainly be helpful in the fabrication of tunable photonics, biosensors, electro-optical memory devices, etc.

Data availability statement

The data that support the findings of this study are available upon reasonable request from the authors.

Acknowledgments

The authors are thankful to Professor Sunita Rattan, Director, Amity Institute of Applied Sciences (AIAS), Amity University Uttar Pradesh (AUUP), Noida for her continuous encouragement and interest in the present study. We are also grateful to AUUP, Noida, for providing the research facilities to carry out the present research work. Priscilla P thanks UGC for the fellowship awarded under the scheme Savitribai Jyotirao Phule Single Girl Child Fellowship (SJSGC 2022-2023). Jai Prakash and Gautam Singh are grateful to the Council of Science and Technology (CST), U. P., India for financial assistance under CST, U. P. funded research project (Project ID: 1960). Authors Supreet, Gautam Singh, Sanjeev Kumar and Praveen Malik acknowledge the support provided under SERB SURE Grant No. SUR/2022/004020 of Govt. of India. Praveen Malik acknowledges the support by CRG-SERB under Grant No. CRG/2022/007362.

ORCID iDs

Jai Prakash https://orcid.org/0000-0002-1100-0749
Sanjeev Kumar https://orcid.org/0000-0002-7560-1973
Riccardo Castagna https://orcid.org/0000-0003-4361-9957
Gautam Singh https://orcid.org/0000-0002-7514-1196

References

[1] Dierking I, Yoshida S, Kelly T and Pitcher W 2020 Liquid crystal–ferrofluid emulsions *Soft Matter* **16** 6021
[2] Collings P J and Hird M 2017 *Introduction to Liquid Crystals: Chemistry and Physics* (CRC Press) (https://doi.org/10.1201/9781315272801)
[3] Demus D 1988 100 years liquid crystal chemistry *Mol. Cryst. Liq. Cryst.* **165** 45–84
[4] Bahadur B 1990 *Liquid Crystals: Applications and Uses* (World Scientific)
[5] Ma L L, Li C Y, Pan J T, Ji Y E, Jiang C, Zheng R, Wang Z Y, Wang Y, Li B X and Lu Y Q 2022 Self-assembled liquid crystal architectures for soft matter photonics *Light Sci. Appl.* **11** 270
[6] Lagerwall J P F and Scalia G 2012 A new era for liquid crystal research: applications of liquid crystals in soft matter nano-, bio- and microtechnology *Curr. Appl. Phys.* **12** 1387
[7] Yin K, Hsiang E L, Zou J, Li Y, Yang Z, Yang Q, Lai P C, Lin C L and Wu S T 2022 Advanced liquid crystal devices for augmented reality and virtual reality displays: principles and applications *Light Sci. Appl.* **11** 161
[8] Li Y L, Li N N, Wang D, Chu F, Lee S D, Zheng Y W and Wang Q H 2022 Tunable liquid crystal grating based holographic 3D display system with wide viewing angle and large size *Light Sci. Appl.* **11** 188
[9] Qi H, Hegmann T, Bruce D W, Goodby J W and Sambles J R 2008 Impact of nanoscale particles and carbon nanotubes on current and future generations of liquid crystal displays *J. Mater. Chem.* **18** 3288
[10] Wang Z, Xu T, Noel A, Chen Y C and Liu T 2021 Applications of liquid crystals in biosensing *Soft Matter* **17** 4675
[11] Zhang Z, Yang X, Zhao Y, Ye F and Shang L 2023 Liquid crystal materials for biomedical applications *Adv. Mater.* **35** 2300220
[12] Kim Y H, Lee J O, Jeong H S, Kim J H, Yoon E K, Yoon D K, Yoon J B and Jung H T 2010 Optically selective microlens photomasks using self-assembled smectic liquid crystal defect arrays *Adv. Mater.* **22** 2416
[13] Serra F, Gharbi M A, Luo Y, Liu I B, Bade N D, Kamien R D, Yang S and Stebe K J 2015 Curvature-driven, one-step assembly of reconfigurable smectic liquid crystal compound eye lenses *Adv. Opt. Mater.* **3** 1287

[14] Ozaki M, Kasano M, Kitasho T, Ganzke D, Haase W and Yoshino K 2003 Electro-tunable liquid-crystal laser *Adv. Mater.* **15** 974

[15] Takeoka Y, Honda M and Seki T 2009 Dual tuning of the photonic band-gap structure in soft photonic crystals *Adv. Mater.* **21** 1801

[16] Son B, Kim S, Kim Y H, Käläntär K, Kim H-M, Jeong H-S, Choi S Q, Shin J, Jung H-T and Lee Y-H 2014 Optical vortex arrays from smectic liquid crystals *Opt. Exp.* **22** 4699

[17] Yang D K and Wu S T 2014 *Fundamentals Of Liquid Crystal Devices* (Wiley)

[18] Malik M, Iqbal M A, Shahid W, Ud Din S Z, Ikram M, Anwar N, Shahid S and Idrees F 2022 Overview of liquid crystal research: computational advancements, challenges, future prospects and applications, liquid crystals IntechOpen

[19] Hegmann T, Qi H and Marx V M 2007 Nanoparticles in liquid crystals: synthesis, self-assembly, defect formation and potential applications *J. Inorg. Organomet. Polym. Mater.* **17** 483

[20] Anu, Varshney D, Yadav K, Prakash J, Meena H and Singh G 2023 Tunable dielectric and memory features of ferroelectric layered pervoskite $Bi_4Ti_3O_{12}$ nanoparticles doped nematic liquid crystal composites *J. Mol. Liq.* **369** 120820

[21] Senyuk B, Glugla D and Smalyukh I I 2013 Rotational and translational diffusion of anisotropic gold nanoparticles in liquid crystals controlled by varying surface anchoring *Phys. Rev.* E **88** 062507

[22] Varshney D, Prakash J and Singh G 2023 Indium tin oxide nanoparticles induced tunable dual alignment in nematic liquid crystal *J. Mol. Liq.* **374** 121264

[23] Soulé E R, Milette J, Reven L and Rey A D 2012 Phase equilibrium and structure formation in gold nanoparticles—nematic liquid crystal composites: experiments and theory *Soft Matter* **8** 2860

[24] Kumar A, Singh D P and Singh G 2022 Recent progress and future perspectives on carbon nanomaterials dispersed liquid crystals composites *J. Phys. D: Appl. Phys.* **55** 083002

[25] Qi H and Hegmann T 2009 Multiple alignment modes for nematic liquid crystals doped with alkylthiol-capped gold nanoparticles *ACS Appl. Mater. Interfaces* **1** 1731

[26] Parveen A, Prakash J and Singh G 2022 Impact of strontium titanate nanoparticles on the dielectric, electro-optical and electrical response of a nematic liquid crystal *J. Mol. Liq.* **354** 118907

[27] Choudhary A, Singh G and Biradar A M 2014 Advances in gold nanoparticle–liquid crystal composites *Nanoscale* **6** 7743

[28] Singh P K, Dhar R and Dabrowski R 2023 Enhancement of dielectric and electrocharacteristics of liquid crystalline material -optical 4′-Octyl-4-Cyano-Biphenyl with dispersed functionalized and nonfunctionalized multiwalled carbon nanotubes *Phys. Rev.* E **107** 044704

[29] Basu R and Iannacchione G S 2010 Orientational coupling enhancement in a carbon nanotube dispersed liquid crystal *Phys. Rev.* E **81** 051705

[30] Kumar A, Priyam, Meena H, Prakash J, Wang L and Singh G 2022 Recent advances on semiconducting nanomaterials-ferroelectric liquid crystals *J. Phys.: Condens. Matter* **34** 013004

[31] Basu R and Iannacchione G S 2009 Nematic anchoring on carbon nanotubes *Appl. Phys. Lett.* **95** 173113

[32] Priscilla P, Malik P, Supreet A K, Castagna R and Singh G 2023 Recent advances and future perspectives on nanoparticles-controlled alignment of liquid crystals for displays and other photonic devices *Crit. Rev. Solid State Mater. Sci.* **48** 57

[33] Goel P, Singh G, Pant R P and Biradar A M 2012 Investigation of dielectric behaviour in ferrofluid-ferroelectric liquid crystal nanocomposites *Liq. Cryst.* **39** 927–32

[34] Chinky, Kumar P, Sharma V, Malik P and Raina K K 2019 Nano particles induced vertical alignment of liquid crystal for display devices with augmented morphological and electro-optical characteristics *J. Mol. Struct.* **1196** 866

[35] Guo Y, Li W, Li X, Zhang H, Ma H and Sun Y 2019 Influences of nickel plated multi-walled carbon-nanotube on the electro-optical properties of nematic liquid crystal *Nanotechnology* **30** 475201

[36] Bukowczan A, Hebda E and Pielichowski K 2021 The influence of nanoparticles on phase formation and stability of liquid crystals and liquid crystalline polymers *J. Mol. Liq.* **321** 114849

[37] Jacak L, Hawrylak P and Wojs A 2013 *Quantum Dots* (Springer)

[38] Maxwell T, Nogueira Campos M G, Smith S, Doomra M, Thwin Z and Santra S 2019 *Nanoparticles for Biomedical Applications: Fundamental Concepts, Biological Interactions and Clinical Applications* (Elsevier Science)

[39] Bourzac K 2013 Quantum dots go on display *Nature* **493** 283

[40] Mirzaei J, Reznikov M and Hegmann T 2012 Quantum dots as liquid crystal dopants *J. Mater. Chem.* **22** 22350

[41] Singh G, Fisch M and Kumar S 2016 Emissivity and electrooptical properties of semiconducting quantum dots/rods and liquid crystal composites: a review *Rep. Prog. Phys.* **79** 056502

[42] Supreet and Singh G 2020 Recent advances on cadmium free quantum dots-liquid crystal nanocomposites *Appl. Mater. Today* **21** 100840

[43] Singh A K, Malik P, Chauhan G, Hegde G and Malik P 2023 Synthesis and characterization of biowaste-based porous carbon nanoparticle-polymer dispersed ferroelectric liquid crystal composites *J. Mol. Liq.* **390** 123024

[44] Liu G, Zhang S, Xu L, Hu Y, Li X, Zhang S and Zeng H 2022 Recent advances of eco-friendly quantum dots light-emitting diodes for display *Prog. Quantum Electron.* **86** 100415

[45] Zhao H *et al* 2021 Gram-scale synthesis of carbon quantum dots with a large stokes shift for the fabrication of eco-friendly and high-efficiency luminescent solar concentrators *Energy Environ. Sci.* **14** 396

[46] Mansuriya B D and Altintas Z 2021 Carbon dots: classification, properties, synthesis, characterization, and applications in health care—an updated review *Nanomaterials* **11** 2525

[47] Liu J, Li R and Yang B 2020 Carbon dots: a new type of carbon-based nanomaterial with wide applications *ACS Cent. Sci.* **6** 2179

[48] Wang X, Feng Y, Dong P and Huang J 2019 A mini review on carbon quantum dots: preparation, properties, and electrocatalytic application *Front. Chem.* **7** 490939

[49] Neha, Singh G, Kumar S, Malik P and Supreet 2023 Recent trends and insights into carbon dots dispersed liquid crystal composites *J. Mol. Liq.* **384** 122225

[50] Eskalen H 2020 Influence of carbon quantum dots on electro–optical performance of nematic liquid crystal *Appl. Phys.* A **126** 708

[51] Rastogi A, Hegde G, Manohar T and Manohar R 2021 Effect of oil palm leaf-based carbon quantum dot on nematic liquid crystal and its electro-optical effects *Liq. Cryst.* **48** 812

[52] Rastogi A, Pandey F P, Parmar A S, Singh S, Hegde G and Manohar R 2021 Effect of carbonaceous oil palm leaf quantum dot dispersion in nematic liquid crystal on zeta potential, optical texture and dielectric properties *J. Nanostruct. Chem.* **11** 527

[53] Yadav K, Pathak G, Agarwal S, Tripathi S, Kumar S, Srivastava A and Manohar R 2023 C Dots dispersed

nematic liquid crystal as tunable retarder *J. Mater. Sci., Mater. Electron.* **34** 1978
[54] Priscilla P *et al* 2023 Eco-friendly carbon dots induced thermally stable vertical alignment in planar anchored nematic liquid crystal *J. Mol. Liq.* **385** 122318
[55] Priscilla P *et al* 2024 Effect of doping of organo-soluble carbon dots on ionic relaxation and conductivity of planar anchored cyanobiphenyl based nematic liquid crystal *J. Mol. Struct.* **1301** 137403
[56] Pandey F P, Rastogi A, Singh S, Pandey F P, Rastogi A and Singh S 2020 Optical properties and zeta potential of carbon quantum dots (CQDs) dispersed nematic liquid crystal 4- Heptyl-4-Biphenylcarbonitrile (7CB) *Opt. Mater.* **105** 109849
[57] Rastogi A, Pandey F P, Hegde G and Manohar R 2020 Time-resolved fluorescence and UV absorbance study on elaeis guineensis/oil palm leaf based carbon nanoparticles doped in nematic liquid crystals *J. Mol. Liq.* **304** 112773
[58] Praseetha K P, Chandrasekharan K and Varghese S 2020 Optical behaviour of nematic liquid crystal doped with carbon dot in the nonlinear optical regime *Opt. Laser Technol.* **130** 106367
[59] Urbanski M, Mirzaei J, Sharma A, Hofmann D, Kitzerow H S and Hegmann T 2016 Chemically and thermally stable, emissive carbon dots as viable alternatives to semiconductor quantum dots for emissive nematic liquid crystal–nanoparticle mixtures with lower threshold voltage *Liq. Cryst.* **43** 183–94
[60] Zheng B, Liu T, Paau M C, Wang M, Liu Y, Liu L, Wu C, Du J, Xiao D and Choi M M F 2015 One pot selective synthesis of water and organic soluble carbon dots with green fluorescence emission *RSC Adv.* **5** 11667–75
[61] Mahesh P, Shah A, Swamynathan K, Singh D P, Douali R and Kumar S 2020 Carbon dot-dispersed hexabutyloxytriphenylene discotic mesogens: structural, morphological and charge transport behavior *J. Mater. Chem.* C **8** 9252
[62] Minervini G, Panniello A, Fanizza E, Agostiano A, Curri M L and Striccoli M 2020 Oil-dispersible green-emitting carbon dots: new insights on a facile and efficient synthesis *Materials* **13** 3716
[63] Haase W and Wrobel S 2003 *Relaxation Phenomena: Liquid Crystals, Magnetic Systems, Polymers, High-Tc Superconductors, Metallic Glasses* (Springer)
[64] Singh G, Vijaya Prakash G, Kaur S, Choudhary A and Biradar A M 2008 Molecular relaxation in homeotropically aligned ferroelectric liquid crystals *Physica* B **403** 3316–9
[65] Singh G, Vijaya Prakash G, Choudhary A and Biradar A M 2010 Homeotropic alignment of nematic liquid crystals with negative dielectric anisotropy *Physica* B **405** 2118–21
[66] Varshney D, Prakash J and Singh G 2023 Indium tin oxide nanoparticles induced molecular rearrangement in nematic liquid crystal material *J. Mol. Liq.* **387** 122578
[67] Neha, Singh G, Malik P, Kumar S, Malik P, Singh A K and Supreet 2023 Tunable optical, electro-optical and dielectric properties of eco-friendly graphene quantum dots-nematic liquid crystal composites *Liq. Cryst.* **50** 2345–59
[68] Urbanski M 2015 On the impact of nanoparticle doping on the electro-optic response of nematic hosts *Liq. Cryst. Today* **24** 102–15
[69] Kinkead B and Hegmann T 2010 Effects of size, capping agent, and concentration of CdSe and CdTe quantum dots doped into a nematic liquid crystal on the optical and electro-optic properties of the final colloidal liquid crystal mixture *J. Mater. Chem.* **20** 448–58
[70] Urbanski M, Mirzaei J, Hegmann T and Kitzerow H S 2014 Nanoparticle doping in nematic liquid crystals: distinction between surface and Bulk effects by numerical simulations *Chem. Phys. Chem.* **15** 1395
[71] Singh P K, Dubey P, Dhar R and Dabrowski R 2023 Improvement in the electro-optical and electronic properties of the reduced graphene oxide dispersed in a liquid crystalline material 4′-octyl-4-cyano-biphenyl *Liq. Cryst.* **50** 476–94
[72] Rani A, Chakraborty S and Sinha A 2021 Effect of CdSe/ZnS quantum dots doping on the ion transport behavior in nematic liquid crystal *J. Mol. Liq.* **342** 117327
[73] Kumar J, Prasad V and Manjunath M 2018 Quantum dots dispersed hockey stick nematic liquid crystal: studies on dielectric permittivity, elastic constants and electrical conductivity *J. Mol. Liq.* **266** 10–18
[74] Urbanski M and Lagerwall J P F 2017 Why organically functionalized nanoparticles increase the electrical conductivity of nematic liquid crystal dispersions *J. Mater. Chem.* C **5** 8802–9
[75] Urbanski M and Lagerwall J P F 2016 Nanoparticles dispersed in liquid crystals: impact on conductivity, low-frequency relaxation and electro-optical performance *J. Mater. Chem.* C **4** 3485–91